A Fractional-Order Wireless Power Transfer System Insensitive to Resonant Frequency

Yanwei Jiang and Bo Zhang, *Senior Member, IEEE*

***Abstract*—Since electric power was first transferred wirelessly by Tesla over a hundred years ago, wireless power transfer (WPT) systems have always been composed of integer-order components, such as inductors and capacitors. Recent studies have shown that efficient WPT can be achieved in the range of tens of centimeters or even meters by using magnetic-coupling of two or more integer-order resonant circuits. However, their transfer efficiency and output power are highly sensitive to the resonant frequency. Unfortunately, the resonant frequency is easily disturbed by metal or nonresistive load and so on in real-world application, which will unavoidably lead to transfer efficiency reduction and unstable output power in these integer-order circuits. Therefore, this article proposes and experimentally demonstrates a fractional-order WPT system containing a fractional-order capacitor, in which the transfer efficiency and output power are inherently stable and insensitive to the resonant frequency. The results show that the efficiency and output power only change within 1% when the receiver resonant frequency is detuned by ±5%. In contrast, the WPT systems that are sensitive to the resonant frequency suffer from fall in the efficiency of around 30%, and a largely unstable output power. The available experiments verify the effectiveness of the proposed system.**

***Index Terms*—Fractional-order, resonant frequency, wireless power transfer (WPT).**

I. Introduction

WIRELESS power transfer (WPT) has been considered to be a promising alternative technology to cable charging, due to the inherent advantages of flexibility, safety, convenience, and galvanic isolation [1]. In recent years, WPT technology has been applied in a large number of civil occasions and promoted to the market, such as portable electronic devices, implantable medical devices, kitchen appliances, electric vehicles, lighting application, and so on [2], [3]. Moreover, WPT technology is also considered to have broad application in industrial fields, such as wireless sensors, automated guided vehicles, automated underwater vehicles, unmanned aerial vehicles, high speed train, and so forth [4], [5].

Manuscript received May 15, 2019; revised July 24, 2019 and September 1, 2019; accepted October 8, 2019. Date of publication October 10, 2019; date of current version February 11, 2020. This work was supported by the Key Program of the National Natural Science Foundation of China under Grant 51437005. Recommended for publication by Associate Editor J. Acero. *(Corresponding author: Bo Zhang.)*

The authors are with the School of Electric Power, South China University of Technology, Guangzhou 510006, China (e-mail: jiang_yanwei@foxmail.com; epbzhang@scut.edu.cn).

Color versions of one or more of the figures in this article are available online at http://ieeexplore.ieee.org.

Digital Object Identifier 10.1109/TPEL.2019.2946964

Power can currently be transferred wirelessly in the far-field or in the near-field. Far-field transfer systems rely on propagating electromagnetic waves and the transfer efficiency is very low if point-to-point transfer is not adopted [6], [7]. Near-field transfer systems operate at distances less than a wavelength of the electromagnetics wave, and have been greatly developed [8]–[18]. Magnetically coupled resonant near-field transfer that consists of two resonant circuits of the same resonant frequency, is very efficient only at a fixed distance, but the efficiency and output power do not remain stable as resonant frequency detunes [8]–[12]. Frequency tracking technology is often used in WPT system to track the operating frequencies that make the source voltage and source current in phase [13], [14] or the source voltage and secondary-side current in phase [15], [16]. By applying frequency tracking technology, the output power or voltage would be constant with variable distances or load, but the transfer efficiency and output power are also unstable when the resonant frequency of transmitter or receiver is detuned. Though recent advances employing a nonlinear parity-time-symmetry circuit can also offer stable efficiency and output power under the variation of the transfer distance [17], [18], the transfer efficiency and output power are also unstable when the resonant frequency of transmitter or receiver varies. Unfortunately, the resonant frequency of wireless power-transfer systems is easily shifted in actual world [8], [19]–[22], for example, in common electromagnetic environment produced by metal objects. In [19], ferrite is used to shield receiver coil to avoid external disturbance to the receiver, but it increases the weight of the receiver and cannot overcome the interference of nonresistive load to the resonant frequency. By retuning the transmitter resonant frequency, two resonators could resonate at same frequency, but requiring the information of the receiver resonant frequency, which is hard to obtain when the resonant frequency is disturbed [22]. Hence, there is a real need and still a fundamental challenge to develop a WPT system capable of maintaining a high efficiency and stable output power when the resonant frequency is disturbed.

To solve this issue, this article proposes a fractional-order WPT system that incorporates a fractional-order capacitor of order bigger than one. Fractional-order capacitor is a kind of capacitor modeled by fractional calculus. In contrast to an integer-order capacitor that is described by first-order calculus, the current–voltage relationship of the fractional-order capacitor is defined as

$$i(t) = C_\alpha \frac{d^\alpha}{dt^\alpha} v(t) \tag{1}$$

where d^{α}/dt^{α} is termed the fractional-order derivative operator, C_{α} is the capacitance value, and α is its order [23], with $\alpha \in$ (0,2). In fact, (1) was initially used to accurately describe the capacitor model, since there is no ideal integer-order capacitor [24]. However, the orders of most capacitors are close to 1, so their fractional-order characteristics are often neglected and treated as 1. Nevertheless, some capacitors have been found to have strong fractional-order properties, such as super-capacitor, its order is much smaller than 1 [25]. Therefore, it is interesting and necessary to study the characteristics of fractional-order capacitor with various orders. The impedance of a fractional-order capacitor can be described as [23]

$$Z_C = \frac{1}{\omega^{\alpha} C_{\alpha}} \cos(0.5\pi\alpha) - j\frac{1}{\omega^{\alpha} C_{\alpha}} \sin(0.5\pi\alpha) \tag{2}$$

where ω is the operating angular frequency, so a fractional-order capacitor contains the capacitor reactance as well as the resistance, which is determined by α. However, the integer-order capacitor, i.e., $\alpha = 1$, only has a capacitor reactance. Moreover, when the order is less than 1, the resistance of fractional-order capacitor is positive, which would bring additional losses to the circuit, and the smaller the order, the greater the loss. When the order α is greater than 1, the resistance of a fractional-order capacitor is negative, which indicates that this capacitor can provide active power. Thus, the fractional-order capacitor with order bigger than 1 is adopted in this article. In addition, the phase angle of fractional-order capacitor is $0.5\pi\alpha$, which is independent of ω and only depends on the order α. Hence, a fractional-order capacitor has the characteristic of constant phase angle.

The application of fractional-order capacitors is also an attractive topic. In recent years, the properties of applying a fractional-order capacitor in dc–dc converters were discussed in [26] and [27], their results show that the output voltage gain depends not only on duty cycle but also on the order of the fractional-order capacitor. The use of fractional-order capacitors in *LC* circuits and impedance matching networks have also been extensively studied in [28]–[31]. The resonant frequency of *LC* circuit depends on the inductance, capacitance, and the fractional-order α, so that the resonant frequency can be controlled easily by multiparameters [28]–[30]. As for impedance matching networks, only a single fractional-order capacitor acts as a capacitance and resistance to match any inductive impedance, so additional resistance is not needed [31]. Therefore, the fractional-order capacitor has demonstrated more design flexibility and beneficial properties than the integer-order capacitor. Inspired by above works, this article uses a fractional-order capacitor to construct a WPT system that can be insensitive to the resonant frequency. Although the fractional-order capacitor is not yet a standard market-oriented component, customized fractional-order capacitors have been fabricated in the laboratory [32]–[36], paving the way for the design of fractional-order capacitors for use in WPT systems.

This article is organized as follows. The operating principle of the proposed fractional-order WPT system is described in Section II. The comparison with other WPT systems is analyzed in Section III. A prototype is built to prove the feasibility of the proposed method and the experimental results on the characteristic of the proposed system are discussed, in Section IV. Section V concludes this article.

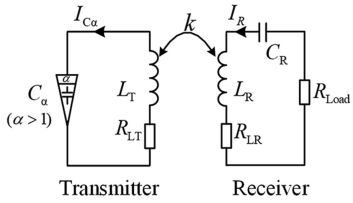

Fig. 1. System structure of the proposed fractional-order WPT system based on a fractional-order capacitor C_{α}.

II. Principles of the Fractional-Order WPT System

A. System Structure

The proposed fractional-order WPT system is shown in Fig. 1. Its transmitter contains a fractional-order capacitor C_{α} with order bigger than 1. The fractional-order capacitor has a fixed order α and its capacitance C_{α} can be changed. Since the fractional-order capacitor has a negative resistance component, power is fed into the transmitter via the fractional-order capacitor before being transferred through coupling to the receiver. The transmitter and receiver are coupled together by inductor L_T and L_R with mutual inductance coefficient k. R_{LT} and R_{LR} represent the internal resistance of the transmitter and receiver, respectively.

From Fig. 1, the transmitter is a resonator, and its resonant frequency ω_T can be expressed as [23]

$$\omega_T = \left[\frac{\sin(0.5\pi\alpha)}{L_T C_{\alpha}}\right]^{\frac{1}{1+\alpha}} \tag{3}$$

while the resonant frequency of the receiver is $\omega_R = [1/(L_R C_R)]^{1/2}$.

B. Modeling Based on Coupled-Mode Theory

To study the performance of the fractional-order WPT system, a coupled-mode theory model of the system is built in this section. According to coupled-mode theory [37], the system model can be described by

$$\frac{d}{dt}\begin{bmatrix} \boldsymbol{a}_T \\ \boldsymbol{a}_R \end{bmatrix} = \begin{bmatrix} j\omega_T + g_T & -j\kappa \\ -j\kappa & j\omega_R - \tau_R \end{bmatrix}\begin{bmatrix} \boldsymbol{a}_T \\ \boldsymbol{a}_R \end{bmatrix} \tag{4}$$

where $\boldsymbol{a}_T$ and $\boldsymbol{a}_R$ are defined as the modal amplitudes, so that the energy stored in the transmitter and receiver are $|\boldsymbol{a}_T|^2$ and $|\boldsymbol{a}_R|^2$ respectively; g_T is the overall gain rate of the transmitter and τ_R is the overall loss rate of the receiver; κ is the coupling rate between the transmitter, and receiver, which is defined as

$$\kappa = \frac{k}{2}\sqrt{\omega_T \omega_R}. \tag{5}$$

From Fig. 1, the overall gain rate g_T of the transmitter depends on the fractional-order capacitor and internal resistance. The gain rate $g_{C\alpha}$ of the fractional-order capacitor can be derived as

$$g_{C\alpha} = \frac{-\cos(0.5\pi\alpha)}{2\omega^{\alpha} L_T C_{\alpha}} \tag{6}$$

and the intrinsic loss rate of transmitter is $\tau_{LT} = R_{LT}/(2L_T)$, so g_T can be expressed as

$$g_T = g_{C\alpha} - \tau_{LT} = \frac{-\cos(0.5\pi\alpha)}{2\omega^{\alpha} L_T C_{\alpha}} - \tau_{LT}. \tag{7}$$

For the receiver, the intrinsic loss rate is $\tau_{LR} = R_{LR}/(2L_R)$ and the load loss rate is $\tau_{\text{Load}} = R_{\text{Load}}/(2L_R)$, so the overall loss rate of the receiver is $\tau_R = \tau_{LR} + \tau_{\text{Load}}$.

C. Analytical Solutions of Operating Frequency

The operating frequency ω of the proposed system can be derived from the steady solutions of the dynamic model of (4). To determine the eigenvalues of (4), we assume $\boldsymbol{A} = (\boldsymbol{a}_T, \boldsymbol{a}_R)^T = (\boldsymbol{A}_T e^{-j\omega t}, \boldsymbol{A}_R e^{-j\omega t})^T$, and have $j\omega\boldsymbol{A} = \boldsymbol{HA}$, where the matrix $\boldsymbol{H}$ is

$$H = \begin{bmatrix} j\omega_T + g_T(\alpha) & -j0.5k\sqrt{(\omega_T\omega_R)} \\ -j0.5k\sqrt{(\omega_T\omega_R)} & j\omega_R - \tau_R \end{bmatrix} \tag{8}$$

According to the eigenvalue equation $\det(\boldsymbol{H} - \omega\boldsymbol{I}) = 0$, and taking ω to be real, the nontrivial solutions of ω can be determined by

$$\begin{cases} (\omega - \omega_T)(\omega - \omega_R) + g_T\tau_R - \frac{k^2}{4}\omega_T\omega_R = 0 \\ (\omega - \omega_T)\tau_R = (\omega - \omega_R) g_T. \end{cases} \tag{9}$$

Using (3), (6), and (7), the expression of g_T can be rewritten as

$$g_T = -\left(\frac{\omega_T}{\omega}\right)^{\alpha+1}\frac{\omega}{2} ctg(0.5\pi\alpha) - \tau_{LT}. \tag{10}$$

By carrying out the first-order Taylor expansion for $(\omega_T/\omega)^{\alpha+1}$, g_T can be approximated as

$$g_T \approx -\left[1 + (\alpha+1)\left(\frac{\omega_T}{\omega} - 1\right)\right]\frac{\omega}{2} ctg(0.5\pi\alpha) - \tau_{LT}. \tag{11}$$

Substituting (11) into (9), we have

$$\begin{aligned} 0 = {} & \omega^3 + \left[X_1 - \left(2 + \frac{\alpha}{4}k^2\right)\omega_R\right]\omega^2 \\ & + \left[\tau_R^2 + \left(1 + \frac{\alpha}{4}k^2\right)\omega_R^2 - X_2 - 2\omega_R\left(1 - \frac{k^2}{8}\right)X_1\right]\omega \\ & + \left[\tau_R^2 + \left(1 - \frac{k^2}{4} - \frac{k^2}{4}\frac{2\tau_R}{\omega_R} tg(0.5\pi\alpha)\right)\omega_R^2 - X_2\right]X_1 \end{aligned} \tag{12}$$

where

$$\begin{cases} X_1 = 2\tau_{LT} tg(0.5\pi\alpha) \\ X_2 = -\dfrac{k^2}{2}\tau_R\omega_R tg(0.5\pi\alpha). \end{cases} \tag{13}$$

In a general WPT system, the mutual inductance coefficient satisfies $k^2 << 1$, and the qualify factor $(Q_R = \omega_R/2\tau_R)$ of the receiver satisfies $1/Q_R << 1$. Meanwhile, the fractional order α is large enough to make sure that $k^2 \text{tg}(0.5\pi\alpha)/4Q_R << 1$. Therefore, (12) can then be approximated as

$$\begin{aligned} 0 \approx {} & \omega^3 + [X_1 - 2\omega_R]\omega^2 \\ & + \left[\tau_R^2 + \omega_R^2 - X_2 - 2\omega_R X_1\right]\omega \\ & + \left[\tau_R^2 + \omega_R^2 - X_2\right]X_1. \end{aligned} \tag{14}$$

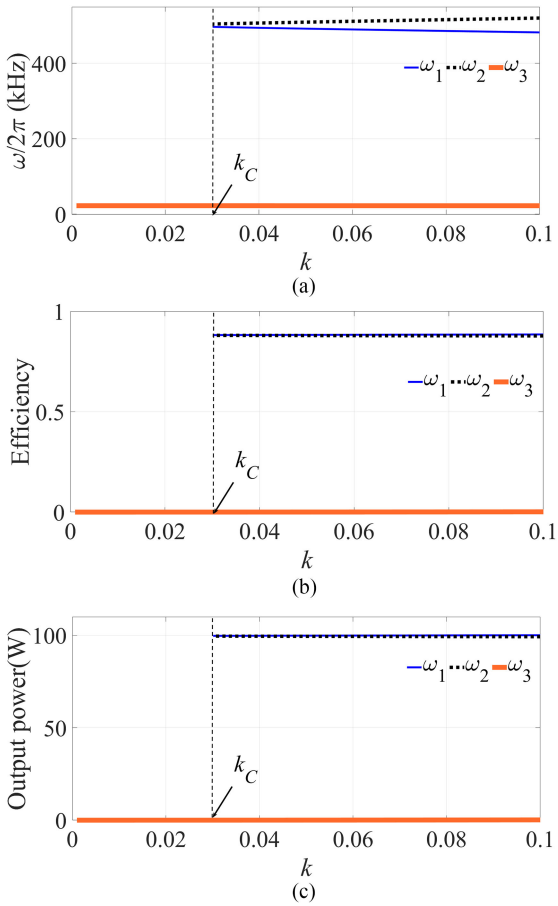

Fig. 2. Curves of (a) system frequency solutions, (b) transfer efficiency and (c) output power as a function of mutual inductance coefficient k.

Factorization of the above equation gives

$$0 = [\omega + X_1]\left[\omega^2 - 2\omega_R\omega + \tau_R^2 + \omega_R^2 - X_2\right]. \tag{15}$$

Thus, three real roots of ω can be found as follows:

$$\omega_{1,2} = \omega_R \pm \sqrt{-\frac{1}{2}k^2\omega_R\tau_R tg(0.5\pi\alpha) - \tau_R^2} \tag{16}$$

$$\omega_3 = -2\tau_{LT} tg(0.5\pi\alpha). \tag{17}$$

From (16) and (17), it can be observed that the solutions of ω are separated into two regions by a critical mutual inductance coefficient k_C, as shown in Fig. 2(a). In the strong coupling region $(k \geq k_C)$, ω has three analytical solutions, ω_1, ω_2, and ω_3, but in the weak coupling region $(k < k_C)$, only one solution, ω_3, exists. According to (16), k_C can be derived as

$$k_C = \sqrt{-\frac{2\tau_R}{\omega_R} ctg(0.5\pi\alpha)}. \tag{18}$$

Based on the equation $\boldsymbol{HA} = j\omega\boldsymbol{A}$, the energy mode ratio can be obtained as

$$\frac{|\boldsymbol{a}_R|^2}{|\boldsymbol{a}_T|^2} = \frac{g_T}{\tau_R} = \frac{\omega - \omega_T}{\omega - \omega_R}. \tag{19}$$

From (9), the resonant frequency ω_T can also be expressed as

$$\omega_T = \frac{\omega\left[(\omega-\omega_R)^2+\tau_R^2\right]}{\left[(\omega-\omega_R)^2+\tau_R^2\right]+0.25k^2\omega_R(\omega-\omega_R)}. \quad (20)$$

The general expression of transfer efficiency η and output power P_o based on coupled-mode theory can be written as

$$\eta = \frac{2\tau_{\rm Load}}{2\tau_R+2\tau_{LT}\left(|\boldsymbol{a}_T|^2/|\boldsymbol{a}_R|^2\right)}. \quad (21)$$

$$P_O = 2\tau_{\rm Load}|\boldsymbol{a}_R|^2. \quad (22)$$

Therefore, using (16)–(22), the transfer efficiency η and output power $P_{\rm o}$ corresponding to the three frequency solutions(ω_1, ω_2, and ω_3) can be solved numerically, as shown in Fig. 2(b) and (c). As can be seen from Fig. 2, the transfer efficiency η is very close to one and output power P_o is almost constant when the frequency solutions are ω_1 or ω_2 in the strong coupling region, but η and $P_{\rm o}$ are close to zero when frequency solutions is ω_3. Thus, ω_1 or ω_2 is selected as the operating frequency of the fractional-order WPT system.

D. Analytical Solutions of Efficiency and Output Power

According to the operating frequency obtained in the previous section, the transfer efficiency and output power of the proposed system are derived in this section.

By substituting into frequency solution $\omega_{1,2}$, (20) can be simplified as

$$\omega_T = \frac{-2\tau_R\omega}{-2\tau_R+(\omega-\omega_R)\,ctg\,(0.5\pi\alpha)}. \quad (23)$$

Then, substituting (10) and (23) into (19), the energy mode ratio can be furthered derived as

$$\frac{|\boldsymbol{a}_{\mathbf{R}}|^2}{|\boldsymbol{a}_T|^2} = -\left(\frac{1+\alpha X_3}{1-X_3}\right)\frac{\omega}{2\tau_R}ctg\,(0.5\pi\alpha_T)-\frac{\tau_{LT}}{\tau_R} \quad (24)$$

where $\mathrm{X}_3=(\omega-\omega_R)/2\tau_R tg(0.5\pi\alpha)$. From (16), $\mathrm{X}_3\approx 0$ when $k^2<<1$, so (24) can be reduced to

$$\frac{|\boldsymbol{a}_R|^2}{|\boldsymbol{a}_T|^2} = -\frac{\omega}{2\tau_R}ctg\,(0.5\pi\alpha)-\frac{\tau_{LT}}{\tau_R}. \quad (25)$$

By substituting (25) into (21), the transfer efficiency of the proposed system can be obtained as follows.

$$\eta = \frac{\tau_{\rm Load}}{\tau_R}\left[1+\frac{1}{Q_{LT}ctg\,(0.5\pi\alpha)+1/\tau_R-1}\right] \quad (26)$$

where $Q_{LT}=\omega/2\tau_{LT}$ is the quality factor of the transmitter coil. τ_R is much larger than one, and Q_{LT} is sufficiently large to make $-Q_{LT}\mathrm{ctg}(0.5\pi\alpha)$ much larger than one, thus (26) can be further reduced to

$$\eta \approx \frac{\tau_{\rm Load}}{\tau_R}\left[1+\frac{1}{Q_{LT}ctg\,(0.5\pi\alpha)}\right]. \quad (27)$$

For the output power $P_{\rm o}$, by substituting (25) into (22), $P_{\rm o}$ can be derived as

$$P_O = -\omega\frac{\tau_{\rm Load}}{\tau_R}\left[ctg\,(0.5\pi\alpha)+\frac{1}{Q_{LT}}\right]|\boldsymbol{a}_T|^2 \quad (28)$$

and

$$|\boldsymbol{a}_T|^2 = \frac{\omega^{\alpha-1}C_\alpha}{\sin\,(0.5\pi\alpha)}V_{C\alpha}^2\sin^2\,(0.5\pi\alpha) = \frac{1}{\omega}S_\alpha\sin\,(0.5\pi\alpha) \quad (29)$$

where $V_{C\alpha}$ and $S_\alpha=\omega^\alpha C_\alpha V_{C\alpha}^2$ are the voltage and apparent power of the fractional-order capacitor, respectively. Using (28) and (29), $P_{\rm o}$ can be expressed as

$$P_O = -\frac{\tau_{\rm Load}}{\tau_R}\left[1+\frac{1}{Q_{LT}ctg\,(0.5\pi\alpha)}\right]S_\alpha\cos\,(0.5\pi\alpha). \quad (30)$$

As can be seen from (27) and (30), the transfer efficiency η and output power P_o are determined only by the order α, the load loss rate $\tau_{\rm Load}$, the receiver loss rate τ_R and the quality factor Q_{LT}. Hence, the fractional-order WPT system can be inherently insensitive to the resonant frequency.

III. Comparison With Other WPT Systems

In this section, the sensitivity of the proposed fractional-order system to resonant frequency is compared with that of magnetically coupled resonant-based wireless power transfer system (MCR-WPT) and parity-time-symmetry circuit-based wireless power transfer (PT-WPT) system. In the analysis below, without loss of generality, assume that only the resonant frequency ω_R of the receiver is disturbed.

Since the order of the fractional-order capacitor is bigger than one, the inverter in transmitter is simultaneously controlled as a negative resistance to provide an ac source, so all switch losses of the inverter are considered as the loss of ac source. In a MCR-WPT system, its loss of ac source is also the switch losses of inverter. In a PT-WPT system, the negative resistance also provides an ac source. Therefore, to ensure the consistency and fairness, the loss of ac source in above three systems are all not considered in the following comparison of transfer efficiency.

For MCR-WPT system, two-coil resonant system is often used [9]–[12], as shown in Fig. 3(a).The input source is generally a high-frequency ac power supply. The transfer efficiency $\eta_{\rm MCR}$ and output power $P_{\rm MCR}$ is described as follows:

$$\eta_{\rm MCR} = \frac{\tau_{\rm Load}\kappa^2}{\tau_{LT}\left[(\tau_{LR}+\tau_{\rm Load})^2+(\omega-\omega_R)^2\right]+(\tau_{LR}+\tau_{\rm Load})\,\kappa^2} \quad (31)$$

$$P_{\rm MCR} = 2\tau_{\rm Load}|\boldsymbol{a}_R|^2 = 2\tau_{\rm Load}\frac{\kappa^2F^2}{\left[\kappa^2+\tau_{LT}\,(\tau_{LR}+\tau_{\rm Load})\right]^2+\left[\tau_{LT}\,(\omega-\omega_R)\right]^2} \quad (32)$$

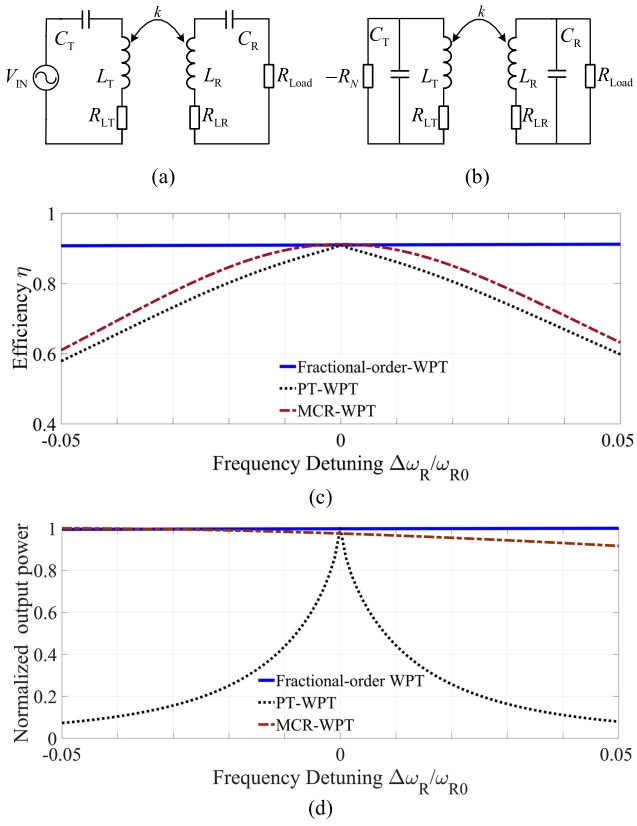

Fig. 3. Comparison with (a) MCR-WPT system and (b) PT-WPT system of (c) transfer efficiency, and (d) normalized output power.

where F and ω are the amplitude and frequency of the input source, respectively. The normalized output power of the resonant system is $P_{\rm MCR}/P_{\rm MAX1}$, where $P_{\rm MAX1}$ is the maximum output power of $P_{\rm MCR}$ during ω_R changes. From (31) and (32), $\eta_{\rm MCR}$ and $P_{\rm MCR}$ are unstable when ω_R varies.

For PT-WPT system [17], a nonlinear negative resistance is used as shown in Fig. 3(b). The transfer efficiency η_{PT} and output power $P_{\rm MCR}$ can be described as follows:

$$\eta_{PT} = \frac{2\tau_{\rm Load}}{2\tau_R + 2\tau_{LT}\left(\frac{\omega-\omega_R}{\omega-\omega_T}\right)} \tag{33}$$

$$P_{PT} = 2\tau_{\rm Load}|\boldsymbol{a}_R|^2 = 2\tau_{\rm Load}\frac{\omega-\omega_T}{\omega-\omega_R}C_T V_{\rm IN}^2 \tag{34}$$

where C_T is the capacitor of the transmitter and $V_{\rm IN}$ is the voltage of the negative resistor. The corresponding normalized output power is $P_{PT}/P_{\rm MAX2}$, where $P_{\rm MAX2}$ is the maximum output power of P_{PT} during ω_R changes. From (33) and (34), the energies of transmitter and receiver are unbalanced when ω_R varies, which result in the unstable transfer efficiency and output power.

Fig. 3(c) and (d) shows the transfer efficiency η and normalized output power under detuning of the receiver resonant frequency in the strong coupling regime with $k = 0.031$. $\Delta\omega_R$ and ω_{R0} are the resonant-frequency detuning and the rated resonant frequency of the receiver, respectively. The resonant frequency ω_T of the transmitter is set to ω_{R0} in MCR-WPT system and PT-WPT system; and the other parameters are the same with the proposed fractional-order system. As can be seen from Fig. 3(c) and (d), MCR-WPT system and PT-WPT system are sensitive to the resonant frequency, but the proposed system is not. To demonstrate the comparison results more clearly, the transfer efficiency and normalized output power of the three WPT systems are also shown in Table I. When the receiver resonant frequency is detuned by $\pm 5\%$, the MCR-WPT system and PT-WPT system have an around 30% drop in transfer efficiency and have a largely unstable output power, but the transfer efficiency and output power of the proposed system only change within 1%.

TABLE I
RESULTS OF COMPARISON OF THE PROPOSED FRACTIONAL-ORDER WPT SYSTEM WITH OTHER WPT SYSTEMS

System	Frequency Detuned	Transfer Efficiency	Normalized Output Power	Sensitiveness
MCR-WPT	+0.05	0.6103	1	Sensitive
	0	0.9121	0.9752	
	-0.05	0.6319	0.9159	
PT-WPT	+0.05	0.5791	0.0729	Sensitive
	0	0.9099	1	
	-0.05	0.5986	0.0794	
Proposed Fractional-order WPT	+0.05	0.9075	0.9951	Insensitive
	0	0.9099	0.9977	
	-0.05	0.912	1	

The MCR-WPT system can also have variable frequency control to make $\omega = \omega_R$ for various ω_R, so that the efficiency also will not vary with respect to detuning, but the premise is that the resonant frequency ω_R of the receiver could be acquired. However, when the receiver is disturbed, it is difficult to accurately obtain the value of ω_R. For the proposed fractional-order WPT system, the transfer efficiency is dependent of the order α, but independent of the resonant frequency ω_R, so we only need to use a fractional-order capacitor with a fixed order in the transmitter, without acquiring the value of ω_R.

IV. Experimental Verification

To practically evaluate the performance of the proposed system, a fractional-order capacitor is constructed and used to build the fractional-order WPT prototype system.

A. Implementation of the Fractional-Order Capacitor

To realize the fractional-order WPT system in practice, the fractional-order capacitor should have distinct characteristics. First, its order α should be a constant and larger than one, but should enable the capacitance to vary within the specified operating frequency band. Second, the capacitor must have a constant apparent power S_α.

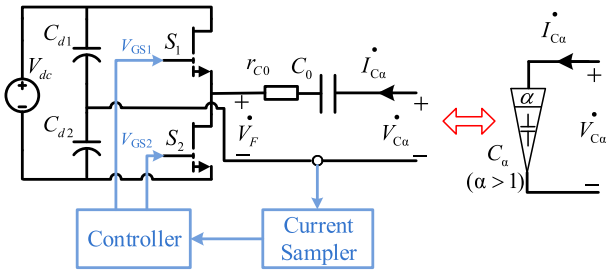

Fig. 4. Circuit diagram of the fractional-order capacitor based on a power electronic converter.

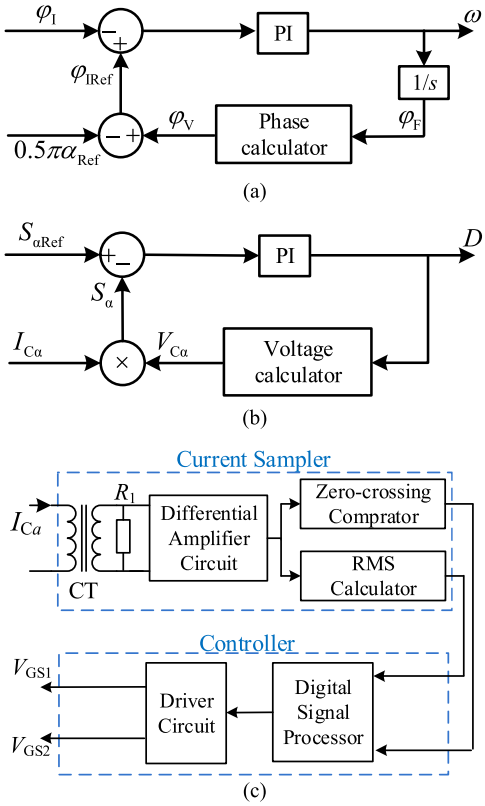

Fig. 5. Control block diagram used to fabricate the fractional-order capacitor. (a) Phase-locked-loop control block diagram. (b) Apparent power control block diagram. (c) The implementation block diagram of the controller and current sampler.

A power electronic converter is used to fabricate the fractional-order capacitor, as shown in Fig. 4. The circuit consists of a half-bridge converter and a capacitor C_0, and r_{C0} is the internal resistance of C_0, S_1 and S_2 are a pair of power switches that turn ON and OFF complementarily, V_{GS1} and V_{GS2} are the drive signal of switch S_1 and S_2, respectively.

A fixed value of order α can be obtained by controlling the phase difference of the input voltage $V_{C\alpha}$ and current $I_{C\alpha}$ constant. A phase-lock loop can be applied to control the phase difference by adjusting the operating frequency ω of resonator [38]. The phase-lock control strategy used in this article is detailed in Fig. 5(a). PI refers to a proportional-integral controller and s is Laplacian Operator. The operation frequency ω is the switching frequency of S_1 and S_2. From (2), the relationship between the order α and the phase difference of input voltage and current can be expressed as

$$\alpha = \frac{\varphi_V - \varphi_I}{0.5\pi} \tag{35}$$

where φ_V and φ_I are the phases of the input voltage $V_{C\alpha}$ and current $I_{C\alpha}$, respectively. Thus, when α_{Ref} is the order that the proposed WPT system needs, the required input current phase is $\varphi_{I\mathrm{Ref}} = \varphi_V - 0.5\pi\alpha_{\mathrm{Ref}}$. The phase φ_I is employed as the feedback of the phase-lock loop and compared with $\varphi_{I\mathrm{Ref}}$. Then, the phase errors are sent to a PI controller, the output of which is the value of the required operating frequency ω.

From Fig. 4, ignoring the internal resistance r_{C0}, the voltage phasor of the fractional-order capacitor can be derived as

$$V_{C\alpha} = V_F + \frac{\sqrt{2}I_{C\alpha}}{\omega C_0}Y_1 + j\frac{\sqrt{2}I_{C\alpha}}{\omega C_0}Y_2 \tag{36}$$

where $Y_1 = \sin(\varphi_I - \varphi_F)$ and $Y_2 = \cos(\varphi_I - \varphi_F)$; $I_{C\alpha}$ is root mean square value of the input current, φ_F and V_F are the phase and amplitude of the output fundamental voltage of the half-bridge circuit. $V_F = (2V_{\mathrm{dc}}/\pi)\sin(D\pi)$, D is the duty of S_1, and φ_F is equal to the phase φ_D of duty D. Thus, the phase φ_V of the input voltage, namely, the phase calculator in Fig. 5(a) can be obtained by

$$\varphi_V = arctg\left(\frac{\sqrt{2}I_{C\alpha}\cos(\varphi_I - \varphi_F)}{\omega C_0 V_F + \sqrt{2}I_{C\alpha}\sin(\varphi_I - \varphi_F)}\right). \tag{37}$$

The apparent power S_α of the fractional-order capacitor can be controlled by adjusting the duty of switch S_1. The control block diagram of S_α is illustrated in Fig. 5(b). The output of the control block is the duty D. From (36), the voltage calculator is

$$V_{C\alpha} = \frac{1}{\sqrt{2}}\sqrt{\left[\frac{2V_{\mathrm{dc}}}{\pi}\sin(D\pi) + \frac{\sqrt{2}I_{C\alpha}}{\omega C_0}Y_1\right]^2 + \left(\frac{\sqrt{2}I_{C\alpha}}{\omega C_0}Y_2\right)^2}. \tag{38}$$

The voltage V_{dc} can be expressed as

$$V_{\mathrm{dc}} = \frac{V_F\pi}{2\sin(D\pi)}. \tag{39}$$

From Fig. 4, the required output fundamental voltage V_F can be deduced as

$$V_F = \sqrt{2\omega^\alpha C_\alpha S_\alpha}\sqrt{\left[\frac{1}{\omega^\alpha C_\alpha}\cos(0.5\pi\alpha)\right]^2 + \left[\frac{1}{\omega^\alpha C_\alpha}\sin(0.5\pi\alpha) - \frac{1}{\omega C_0}\right]^2} \tag{40}$$

From (3) and (23), the steady solutions of the capacitance C_α are derived as

$$C_\alpha = \frac{\sin(0.5\pi\alpha)}{L_T}\left[\frac{-2\tau_R\omega}{-2\tau_R + (\omega - \omega_R)\,ctg\,(0.5\pi\alpha)}\right]^{-1-\alpha}. \tag{41}$$

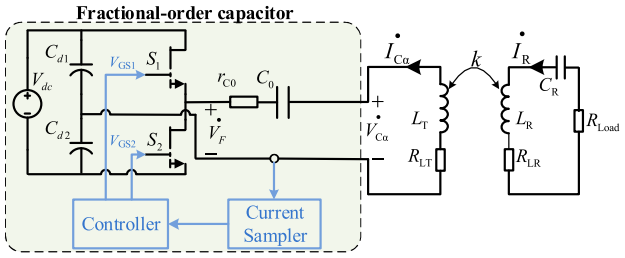

Fig. 6. Full-circuit diagram of the proposed fractional-order WPT system.

Therefore, according to (16) and (39)–(41), the required minimum voltage $V_{\rm dc}$ can be obtained.

The realization of the controller and current sampler in Fig. 4 is based on the block diagram of Fig. 5(c). The current of fractional-order capacitor is converted into voltage signal by a current transformer (CT) CU8965, and then the voltage signal is sampled by a differential amplifier circuit consisting of a high speed operational amplifier OPA2690. The output signal of the differential amplifier circuit passes through a zero-crossing comparator that comprises a high speed comparator TL3016 and an rms calculator AD637, respectively, so a floating-point digital-signal processor TMS320F28377D can sample the rms value and the phase of the capacitor current. The processor processes the sampled signal according to the order control and the apparent power control algorithm, and outputs a pulsewidth modulation wave which is fed into a drive circuit to generator the driving signal $V_{\rm GS1}$ of switch S_1 and the driving signal $V_{\rm GS2}$ of switch S_2. The drive circuit is consist of a dead time generation circuit [18] and two isolated gate drivers (Si8271). The switch S_1 and S_2 are enhancement mode GaN-on silicon power transistors GS66508B.

B. Experimental Results

The full-circuit diagram of the proposed fractional-order WPT system is shown in Fig. 6. The transmitter and receiver coils are wound on two cylindrical acrylic boards and hung on two movable triangular wooden frames as shown in Fig. 7. The two coils are both twined by ten turns of hollow copper wire with an outer diameter of 8 mm and an inner diameter of 6.8 mm, and the diameter of each coil is 60 cm. When the distance between the transmitter and receiver changes the variation of the mutual inductance coefficient is shown in the Fig. 8. All main parameters of the system are given in Table II. From (18) and (27), the higher the order, the higher the efficiency and the smaller the strong coupling region, so the trade-off between efficiency and transfer distance should be considered when choosing the order α. The critical mutual inductance coefficients, the corresponding critical distances and transfer efficiencies of the proposed system for various orders are given in Table III. To maintain more than 90% transfer efficiency within 58 cm, the order α is set to 1.02 in the prototype. As for the selection of S_α, it depends on the required output power $P_{\rm o}$ according to (30).

The measurement approaches of the transfer efficiency and output power of the system are given as follows. First, to

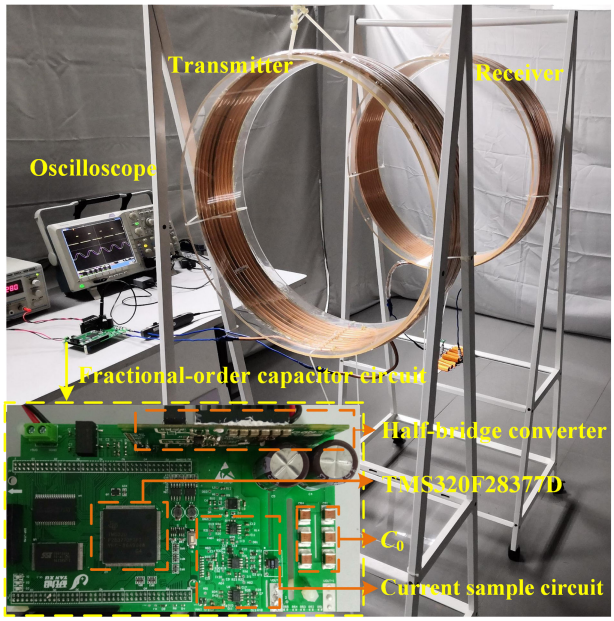

Fig. 7. Photo of the experimental power-transfer prototype system.

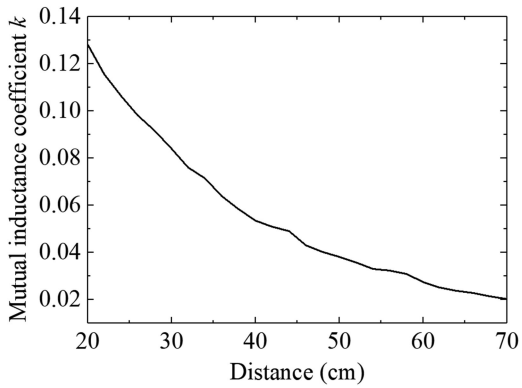

Fig. 8. Measured mutual inductance coefficient k as a function of the distance between the two coaxially aligned coils.

acquire the values of R_{LT} and R_{LR}, an impedance analyzer (Wayne Kerr 6500B) is used to measure the internal resistance of the capacitor, and an reflection measurement method [39] is adopted to measure the quality factor of the transmitter coil and receiver coil to obtain the internal resistance of the coils. Second, the value of the load resistance $R_{\rm Load}$ is also measured by the impedance analyzer. Finally, a current probe (Cybertek CP0030H) and an oscilloscope (Tektronix DPO 4043B) are used to measure the transmitter current $I_{C\alpha}$ and receiver current I_R. Then, the output power can be obtained using the relation $P_O = I_R^2 R_{\rm Load}$, and the transfer efficiency can be obtained using $\eta = I_R^2 R_{\rm Load}/[I_R^2(R_{\rm Load} + R_{LR}) + I_{C\alpha}^2 R_{LT}]$.

When the resonant frequency ω_R of the receiver is equal to the rated resonant frequency ω_{R0}, the transfer efficiency η and output power P_o are measured and the experimental curves are shown in Fig. 9(a), (b). As can be seen from Fig. 9(a), (b), transfer efficiency η, and P_o remain constant within a range of 58 cm.

TABLE II
PARAMETERS FOR THE PROTOTYPE CIRCUIT

Description	Value
Transmitter inductance (L_T)	94.4 μH
Receiver inductance (L_R)	93.6 μH
Resistance (R_{LT})	0.42 Ω
Resistance (R_{LR})	0.42 Ω
Rated-receiver resonant frequency ($\omega_{R0}/2\pi$)	500 kHz
Order of fractional-order capacitor (α)	1.02
Apparent power of fractional-order capacitor (S_a)	3600 VA
DC side voltage (V_{dc})	280 V
Capacitance (C_0)	1.07 nF
Load resistance (R_{Load})	8.45 Ω

TABLE III
CRITICAL MUTUAL INDUCTANCE COEFFICIENTS AND TRANSFER EFFICIENCIES WITH VARIOUS ORDERS

Order α	k_C	Distance (cm)	Efficiency
1.01	0.0218	68	0.8668
1.015	0.0267	62	0.8954
1.02	0.0308	58	0.9097
1.025	0.0344	54	0.9183
1.03	0.0377	51	0.9240
1.035	0.0407	48	0.9281
1.04	0.0436	46	0.9312
1.045	0.0462	45	0.9336
1.05	0.0487	44	0.9355

When the receiver capacitance C_R is changed to simulate the disturbance of ω_R, the transfer efficiency, and output power are also stable, as shown in Fig. 10(a) and (b). The experimental waveforms of voltage $V_{C\alpha}$ and current $I_{C\alpha}$ are shown in Fig. 11. As shown in Fig. 11, the current $I_{C\alpha}$ has a leading time of 520 ns from the voltage $V_{C\alpha}$, and the operating frequency is 491.6 kHz, so the phase of current lead voltage can be obtained as 92.02°. Thus, the actual order of the fractional-order capacitor is $\alpha = 92.02°/90 = 1.0225$. The actual order α has a little deviation from the reference $\alpha_{\text{Ref}} = 1.02$. The main reason is that the phase-lock control strategy is based on that the voltage $V_{C\alpha}$ and current $I_{C\alpha}$ are sinusoidal waves, but the practical voltage and current are not ideal sinusoidal waves. Nevertheless, the relative error of the order is only 0.245%.

Fig. 12 shows the experimental waveforms of transmitter current $I_{C\alpha}$ and receiver current I_R under different detuning of the receiver resonant frequency. From Fig. 12, current $I_{C\alpha}$ and I_R remain unchanged even when the receiver resonant frequency is detuned. These experimental results are consistent with those obtained from coupled-mode theory calculations, and demonstrate successful WPT in which the transfer efficiency and output power are insensitive to the resonant frequency ω_R of the receiver. Although the allowable frequency detuning $\Delta\omega_R/\omega_{R0}$ is 5% in the experiment, this range can be expanded by fabricating a wider bandwidth fractional-order capacitor. Otherwise, the transfer efficiency and output power are insensitive to the resonant frequency only in the strong coupling region that is $k \leq k_C$. In fact, most of WPT systems work in the strong coupling region due to low efficiency in the weak coupling region, even if the resonant frequency is not detuned.

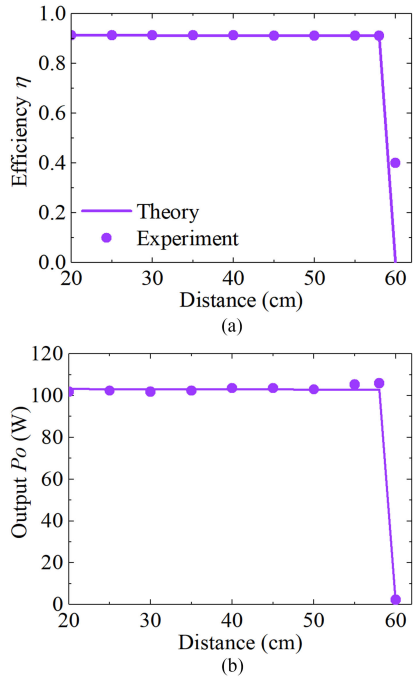

Fig. 9. Experimental results showing the (a) efficiency and (b) output power P_O as a function of distance between transmitter and receiver without receiver resonant frequency detuning.

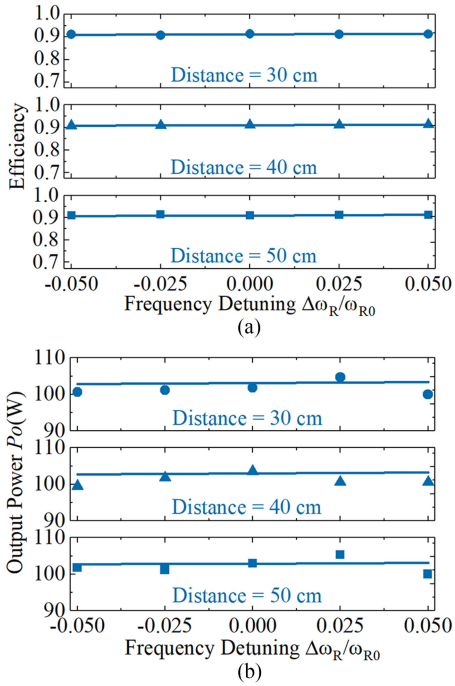

Fig. 10. Experimental results showing the (a) efficiency and (b) output power as a function of receiver resonant frequency detuning.

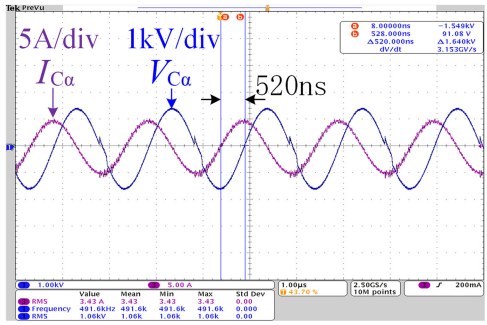

Fig. 11. Experimental waveforms of input voltage and current of fractional-order capacitor.

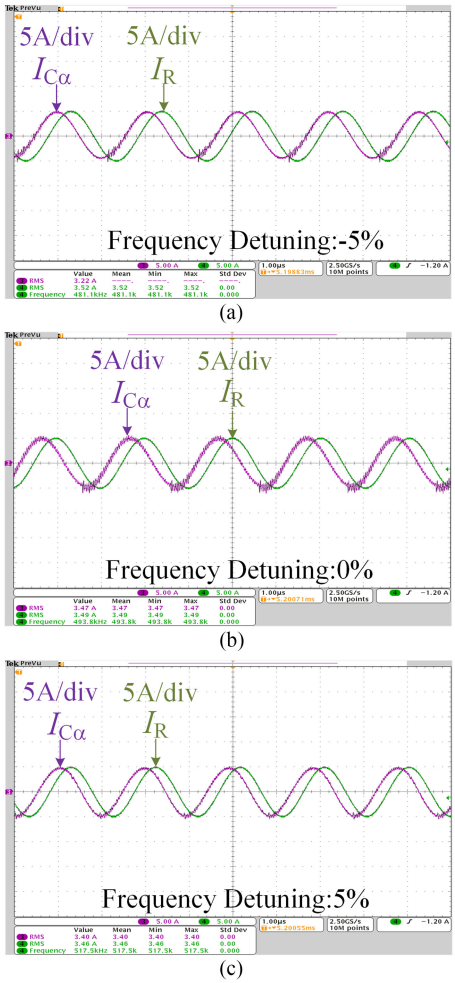

Fig. 12. Experimental transmitter and receiver current waveforms at 50 cm between the two coils. (a). With –5% detuning. (b). Without detuning (c). With 5% detuning.

V. Conclusion

This article proposed a fractional-order wireless power-transfer system that employs a fractional-order capacitor with the order larger than one. By using coupled-mode theory, the analytic solutions of operating frequency, transfer efficiency and output power of the proposed system are derived. Theoretical results show that the system can be insensitive to changes in the receiver's resonant frequency and distance from the transmitter in the strong coupling region. Moreover, this insensitivity depends only on the fractional-order capacitor in the transmitter without adjusting any parameters of the receiver. The experimental results confirm the theoretical analysis. Therefore, the proposed system can allow WPT to be used in any situations where the resonant frequency is easily detuned. In addition, this article may open up a new way for theoretical research and engineering applications of fractional-order energy storage components and systems.

References

[1] Z. Zhang, H. Pang, A. Georgiadis, and C. Cecati, "Wireless power transfer–An overview," *IEEE Trans. Ind. Electron.*, vol. 66, no. 2, pp. 1044–1058, Feb. 2019.

[2] S. Tang, T. Lun, Z. Guo, K. Kwok, and N. McDannold, "Intermediate range wireless power transfer with segmented coil transmitters for implantable heart pumps," *IEEE Trans. Power Electron.*, vol. 32, no. 5, pp. 3844–3857, May 2017.

[3] S. Nutwong, A. Sangswang, S. Naetiladdanon, and E. Mujjalinvimut, "A novel output power control of wireless powering kitchen appliance system with free-positioning feature," *Energies*, vol. 11, no. 7, Jun. 2018, Art. no. 1671.

[4] T. Orekan, P. Zhang, and C. Shih, "Analysis, design, and maximum power-efficiency tracking for undersea wireless power transfer," *IEEE J. Emerg. Sel. Top. Power Electron.*, vol. 6, no. 2, pp. 843–854, Jun. 2018.

[5] J. Kim *et al.*, "Development of 1-MW inductive power transfer system for a high-speed train," *IEEE Trans. Ind. Electron.*, vol. 62, no. 10, pp. 6242–6250, Oct. 2015.

[6] S. Bernd and C. Kai, "Microwave power transmission: Historical milestones and system components," *Proc. IEEE.*, vol. 101, no. 6, pp. 1379–1396, Jun. 2013.

[7] M. Xia and A. Sonia, "On the efficiency of far-field wireless power transfer," *IEEE Trans. Signal Process.*, vol. 63, no. 11, pp. 2835–2847, Jun. 2015.

[8] A. Kurs, A. Karalis, R. Moffatt, J. D. Joannopoulos, P. Fisher, and M. Soljacic, "Wireless power transfer via strongly coupled magnetic," *Science*, vol. 317, no. 5834, pp. 83–86, Jul. 2007.

[9] K. Mehdi and G. Maysam, "The circuit theory behind coupled-mode magnetic resonance-based wireless power transmission," *IEEE Trans. Circuits Syst. I, Regul. Pap.*, vol. 59, no. 9, pp. 2065–2074, Sep. 2012.

[10] Y. Zhang and Z. Zhao, "Frequency splitting analysis of two-coil resonant wireless power transfer," *IEEE Antennas Wirel. Propag. Lett.*, vol. 13, pp. 400–402, Feb. 2014.

[11] H. Y. Lee and G. S. Park, "Analysis of the resonance characteristics by a variation of coil distance in magnetic resonant wireless power transmission," *IEEE Trans. Magn.*, vol. 54, no. 11, Nov. 2018, Art no. 8001704.

[12] H. Feng, T. Cai, S. Duan, X. Zhang, H. Hu, and J. Niu, "A dual-side-detuned series–series compensated resonant converter for wide charging region in a wireless power transfer system," *IEEE Trans. Ind. Electron.*, vol. 65, no. 3, pp. 2177–2188, Mar. 2018.

[13] A. P. Sample, D. A. Meyer, and J. R. Smith, "Analysis, experimental results, and range adaptation of magnetically coupled resonators for wireless power transfer," *IEEE Trans. Ind. Electron.*, vol. 58, no. 2, pp. 544–554, Feb. 2011.

[14] S. Samanta and A. K. Rathore, "Analysis and design of load-independent ZPA operation for P/S, PS/S, P/SP, and PS/SP tank networks in IPT applications," *IEEE Trans. Power Electron.*, vol. 33, no. 8, pp. 6476–6482, Jan. 2018.

[15] K. Yan, Q. Chen, J. Hou, X. Ren, and X. Ruan, "Self-oscillating contactless resonant converter with phase detection contactless current transformer," *IEEE Trans. Power Electron.*, vol. 29, no. 8, pp. 4438–4449, Aug. 2014.

[16] E. Gati, G. Kampitsis, and S. Manias, "Variable frequency controller for inductive power transfer in dynamic conditions," *IEEE Trans. Power Electron.*, vol. 32, no. 2, pp. 1684–1696, Feb. 2017.

[17] A. Sid, X. Yu and S. H. Fan, "Robust wireless power transfer using a nonlinear parity-time-symmetric circuit," *Nature*, vol. 546, no. 7658, pp. 387–390, Jun. 2017.

[18] J. Zhou, B. Zhang, W. Xiao, D. Qiu, and Y. Chen, "Nonlinear parity-time-symmetric model for constant efficiency wireless power transfer: Application to a drone-in-flight wireless charging platform," *IEEE Trans. Ind. Electron.*, vol. 66, no. 5, pp. 4097–4107, May 2019.
[19] L. Tan *et al.*, "Analysis and performance improvement of WPT systems in the environment of single non-ferromagnetic metal plates," *Energies*, vol. 9, no. 576, pp. 1–16, Jul. 2016.
[20] P. Zhang, Q. Yang, X. Zhang, Y. Li, and Y. J. Li, "Comparative study of metal obstacle variations in disturbing wireless power transmission system," *IEEE Trans. Magn.*, vol. 53, no. 6, Jun. 2017, Art no. 9100304.
[21] W. Lee, H. S. Jang, K. S. Oh, and J. W. Yu, "Close proximity effects of metallic environments on the antiparallel resonant coil for near-field powering," *IEEE Trans. Antennas Propag.*, vol. 61, no. 6, pp. 3400–3403, Jun. 2013.
[22] X. Yu *et al.*, "Wireless power transfer in the presence of metallic plates: Experimental results," *AIP Adv.*, vol. 3, Jun. 2013, Art. no. 062102.
[23] A. G. Radwan, "Resonance and quality factor of the RLαCα fractional circuit," *IEEE J. Emerg. Sel. Topics Circuits Syst.*, vol. 3, no. 3, pp. 377–385, Sep. 2013.
[24] S. Westerlund and L. Ekstam, "Capacitor theory," *IEEE Trans. Dielectr. Electr. Insul.*, vol. 1, no. 5, pp. 826–839, Oct. 1994.
[25] T. J. Freeborn, B. Maundy, and A. S. Elwakil, "Measurement of supercapacitor fractional-order model parameters from voltage-excited step response," *IEEE J. Emerg. Sel. Topics Circuits Syst.*, vol. 3, no. 3, pp. 367–376, Jul. 2013.
[26] X. Chen, Y. Chen, B. Zhang, and D. Qiu, "A method of modeling and analysis for fractional-order DC-DC converters," *IEEE Trans. Power Electron*, vol. 32, no. 9, pp. 7034–7044, Sep. 2017.
[27] F. Wang and X. Ma, "Modeling and analysis of the fractional order buck converter in DCM operation by using fractional calculus and circuit averaging technique," *J. Power Electron.*,vol. 13, no. 6, pp. 1008–1015, Nov. 2013.
[28] T.J. Freeborn, B. Maundy, and A. Elwakil, "Fractional resonance-based $RL_\beta C_\alpha$ filters," *Math. Probl. Eng.*, vol. 2013, Jan. 2013, Art. no. 726721.
[29] J. F Gómez-Aguilar, A. Abdon, and V. F. Morales-Delgado, "Electrical circuits RC, LC, and RL described by Atangana–Baleanu fractional derivatives," *Int. J. Circuit Theory Appl.*, vol. 45, pp. 1514–1533, Apr. 2017.
[30] P. Ahmadi, B. Maundy, A. Elwakil, and L. Belostotski, "High-quality factor asymmetric-slope band-pass filters: A fractional-order capacitor approach," *IET Circ. Devices Syst.*, vol. 6, no. 3, pp. 187–197, 2012.
[31] A. G. Radwan, A. Shamim, and K. N. Salama, "Theory of fractional order elements based impedance matching networks," *IEEE Microw. Wirel. Compon. Lett.*, vol. 21, no. 3, pp. 120–122, Mar. 2011.
[32] G. Carlson and C. Halijak, "Approximation of fractional capacitors (1/s)^(1/n) by a regular newton process," *IEEE Trans. Circuit Theory*, vol. 11, no. 2, pp. 210–213, Jun. 1964.
[33] D. Mondal and K. Biswas, "Packaging of single-component fractional-order element," *IEEE Trans. Device Mater. Reliab.*, vol. 13, no. 1, pp. 73–80, Mar. 2013.
[34] G. Tsirimokou, C. Psychalinos, A. S. Elwakil, and K. N. Salama, "Experimental verification of on-chip CMOS fractional-order capacitor emulators," *Electron. Lett.*, vol. 52, no. 15, pp. 1298–1300, Jul. 2016.
[35] A. Adhikary, P. Sen, S. Sen, and K. Biswas, "Design and performance study of dynamic fractors in any of the four quadrants," *Circuits Syst. Signal Process.*, vol. 35, pp. 1909–1932, Dec. 2015.
[36] Y. Jiang and B. Zhang, "High-Power fractional-order capacitor with $1 < \alpha < 2$ based on power electronics," *IEEE Trans. Ind. Electron.*, vol. 65, no. 4, pp. 3157–3164, Apr. 2018.
[37] H. A. Haus, *Waves and Fields in Optoelectronics*. Englewood Cliffs, NJ, USA: Prentice-Hall, 1984, pp. 197–228.
[38] F. M. Gardner. *Phase Lock Techniques*. Hoboken, NJ, USA: Wiley, 2005.
[39] D. Kajfez. *Q Factor Measurements Using MATLAB*. Boston, MA, USA: Artech House, 2011, pp. 81–94.

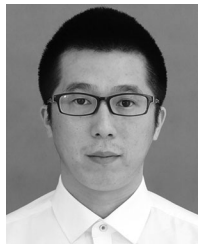

Yanwei Jiang received the B.S. degree in electrical engineering and the M.S.degree in control theory and control engineering from Fuzhou University, Fuzhou, China, in 2012 and 2015, respectively. He is currently working toward the Ph.D. degree in power electronics with the School of Electric Power, South China University of Technology, Guangzhou, China.

His research interests include wireless power transfer applications, power electronics converters, and fractional-order system.

Bo Zhang (M'03–SM'15) was born in Shanghai, China, in 1962. He received the B.S. degree in electrical engineering from Zhejiang University, Hangzhou, China, in 1982, the M.S. degree in power electronics from Southwest Jiaotong University, Chengdu, China, in 1988, and the Ph.D. degree in power electronics from the Nanjing University of Aeronautics and Astronautics, Nanjing, China, in 1994.

He is currently a Professor with the School of Electric Power, South China University of Technology, Guangzhou, China. He has authored or coauthored more than 450 papers and holds 102 patents. He has authored eight monographs. His research interests include nonlinear analysis and control of power electronics, wireless power transfer technology, and ac drives.